

## Conference Paper

# Geometric Accuracy Assessments of Orthophoto Production from UAV Aerial Images

Silvester S. Sai<sup>1</sup>, Martinus E. Tjahjadi<sup>1</sup>, and Catur A. Rokhmana<sup>2</sup><sup>1</sup>Department of Geodesy, National Institute of technology (ITN Malang), Indonesia<sup>2</sup>Department of Geodetic Engineering, Gadjah Mada University, Indonesia

## Abstract

Orthophoto mosaic is assembled from aerial perspective images through a process called orthorectification, which eliminate photographic tilts and terrain relief effects. These orthorectified images have been resampled from the original ones that may have been prepared from a DTM which does not accurately model the surface. Meanwhile, some proprietary software such as Agisoft utilizes spatially dense 3D point clouds that are generated from a so called Structure from Motion technique to generate the orthophoto. The software provides a black-box method to regard these clouds as DSM, and it utilizes this surface model to project pixels from the original images. This paper investigates geometric accuracy of the produced orthophoto mosaic according to the American Society of Photogrammetry and Remote Sensing (ASPRS) standards. To minimize scale differences among images, a 35mm fixed-lens camera is mounted on a fixed-wing UAV platform. Flight missions are carried out at around 250m flying height controlled by a navigational grade sensor on board to provide spatial resolution of about 27mm. A number of orthophoto mosaics are produced by varying number of GCPs, flight paths configuration and terrain relief differences. The geometric accuracies are assessed through a provision of ICPs on each test field area. Coordinates deviations between the ICP and the corresponding orthophotos are framed into a RMSE figures. Within a 95% confidence level, it is revealed that a suitable orthophoto map scale is up to around 1:500. It is recommended that a cross flight configuration to achieve better results.

**Keywords:** UAV, Orthophotomap, ASPRS standard, Accuracy

Corresponding Author:

Silvester S. Sai  
silvester@lecturer.itn.ac.id

Received: 2 August 2019

Accepted: 26 November 2019

Published: 26 December 2019

Publishing services provided by  
Knowledge E

© Silvester S. Sai et al. This article is distributed under the terms of the [Creative Commons Attribution License](#), which permits unrestricted use and redistribution provided that the original author and source are credited.

Selection and Peer-review under the responsibility of the GEODETA 2019 Conference Committee.

## 1. Introduction

An orthophoto is an image of features in their true orthographic position through a process called differential rectification or orthorectification [1--5]. Perspective images photographed from flying Unmanned Aerial Vehicle (UAV) contain displacements in features position due to such factors as sensor motions and lens distortion [6--10], perspective effects (i.e. relief displacement and scale variations), and terrain relief (i.e. scale variations). When the image is rectified into the equivalent vertical image [11, 12],

### OPEN ACCESS

it will remove some displacements caused by tilt (e.g. scale variations) but not relief displacement [1, 3]. In orthorectification, the image is projected onto the DTM so that errors from relief displacement and scale variation due to terrain relief are removed or minimized [2, 13]. A drawback of the orthorectified image is that it cannot model the positions of elevated features such as buildings and bridges. The DTM being used contains elevations of ground points only, all elevations higher than the ground surface may appear incorrectly on the orthorectified image [13].

An orthophoto that accurately portray horizontal positions of elevated features is termed as true orthophoto [14–17]. It utilizes digital surface model (DSM) [16, 17] or digital building model (DBM) [18] to correctly model the elevated features such as man-made structures on the orthorectified image. The true orthophoto still suffers immaterial artifacts like be occluded area behind buildings or bridges, and an occurrence of a visible radiometric differences when there is an attempt to fill such occluded area with different image from different viewpoint [3, 18]. Those artifacts may cause color variations around seamlines of adjacent images taken at different time or from different view point when mosaicking the orthophotos [19]. The resulted orthophoto mosaic will be radiometrically balanced [20, 21] and digitally blended [22, 23] to make the seamlines invisible between overlapping images.

The availability of orthophoto mosaic or orthophoto map at high spatial resolutions is increasingly important for large scale topographic mapping [19] and cadastral mapping [24, 25]. The use of consumer grade cameras mounted on UAV coupled with a so called structure from motion (SfM) method is widely applied for orthophoto productions [26, 27]. SfM automates a computation of Interior Orientation (IO) parameter, and lens distortion of the camera [6, 8], and Exterior Orientation (EO) parameters of all images without the need of known 3D coordinates of control points. It also incorporates Multi-View Stereopsis (MVS) method to derive dense point clouds from overlapping aerial images acquired from multiple altitudes, locations and view angles [28, 29]. Hence, an overall objective of the present research is to evaluate accuracy in an orthophoto obtained by using Sony alpha a5100 camera with a wide angle 35mm fixed length lens mounted on a fixed-wing UAV taking into account a standard test used by ASPRS [30] when the orthophoto is generated by an aforementioned method for over a relatively flat terrain as well as over a rugged and mountainous terrain. The paper is organized as follows: a method comprises theoretical and practical implementation of developing orthophoto, results and discussion, and conclusion.

## 2. Method

### 2.1. Theoretical Concept of Orthophoto

Orthophoto is produced by first generating a DSM from point clouds resulted from the SfM and MVS processes. The DSM is then used to remove relief displacement from the perspective image. The objective of orthorectification is an assignment of color intensity value from the perspective image to each pixel of the DSM. After the rectification, the elevation (Z) and intensity value are stored at the same (x, y) location (Figure1). Collinearity equations are then applied to determine the intensity values as follows,

$$x-x_0 - \Delta x = -c \frac{r_{11}(X - Xc) + r_{12}(Y - Yc) + r_{13}(Z - Zc)}{r_{31}(X - Xc) + r_{32}(Y - Yc) + r_{33}(Z - Zc)} = f_x(X', y') \quad (1)$$

$$y-y_0 - \Delta y = -c \frac{r_{21}(X - Xc) + r_{22}(Y - Yc) + r_{23}(Z - Zc)}{r_{31}(X - Xc) + r_{32}(Y - Yc) + r_{33}(Z - Zc)} = f_y(X', y') \quad (2)$$

The DSM coordinates (X, Y, Z) defined by the DSM pixel are transformed into the perspective image by (1) and (2). Then the color intensity value is interpolated by one of the resampling methods at the image position (x, y), and it is stored at the X, Y position of the orthophoto, which is equal to the position of the DSM point (Figure 1a). Finally, orthogonal or a perpendicular parallel projection is applied to transform the intensity value at the X, Y into the x', y' position on the orthophoto (Figure 1). To perform this transformation, the camera IO parameters of (x<sub>0</sub>, y<sub>0</sub>, c) must be known. The transformation accuracy can be further improved by including lens distortion model (Δx, Δy) into the collinearity equation of (1). This is the case since consumer grade cameras are utilized for aerial photographing, as their lenses are of lower quality than those of metric cameras [6, 8]. The coefficients implemented are correcting radial distortions, decentring distortions, as well as affinities. Other parameters that must also be known are the EO parameters of each image, and pixel intervals. The EO parameters consisting the camera position while taking the image or its perspective center of (X<sub>C</sub>, Y<sub>C</sub>, Z<sub>C</sub>) and a rotation matrix R composed of ω, φ, κ - rotation angles are determined in bundle adjustment computation or using other robust methods such as a single image resection [31-33] and relative orientation [34, 35]. Furthermore, all of the pixel spacing in a metric unit of the digital camera, the DSM cell-size in ground unit, as well as the bounding box rectangle of the DSM pixels in a map projection grid must be determined in advanced.

Orthophoto mosaic is often produced from more than one source image to obtain the required coverage of mapping area (Figure 1b). When the stitched orthophotos contains features of elevated man-made object such as buildings, sometimes the object will be

rectified to a wrong position on the orthophoto mosaic. It is essential to build up high quality DSM, since the point clouds data source of the DSM which generated by the SfM and MVS are still contaminated by random noises. Therefore, to ascertain the quality of the generated orthophoto mosaic obtained from the noisy DSM, a positional accuracy assessment is conducted by implementing the ASPRS Positional accuracy Standards for Digital Geospatial Data. This standard was developed by the ASPRS Map Accuracy Standards Working Group for a purpose of reviewing and updating digital map accuracy standards to conform with state-of-the-art current technologies [30]. In this standard, a new relationship between the imagery Ground Sampling Distance (GSD) derived from digital sensors and the product accuracy (e.g. orthophoto mosaic) is accounted for.

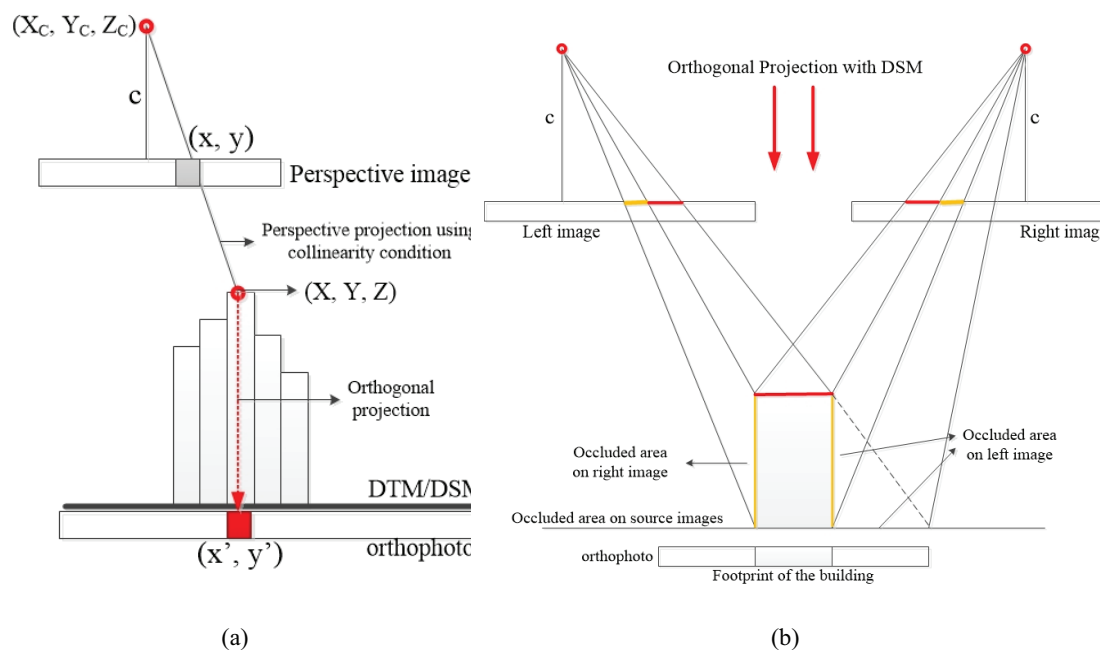


**Figure 1:** Orthorectification process: (a), each 3D surface point defined as pixel of the DSM is transformed into the image the color intensity value from the source image. This value is assigned to the orthophoto raster at the same pixel location as the DSM point. (b), scheme of orthophoto mosaicking: occlusion area in left image can be filled by using image contents from right image.

## 2.2. Camera Lens Specifications and System Configuration

This research is a part of the large scale aerial mapping project using a fixed-wing UAV to map Lowokwaru district in Malang City with its area spanned around 5000Ha [19]. This project uses entry-level consumer grade Sony a5100 camera equipped with an interchangeable lens system, a wide-angle 35mm FFL attached to the camera body [6, 8]. Specifications of the camera system are illustrated in Table 1 as follows.

TABLE 1: Main specification of the mirrorless Sony a5100 compact camera and the replaceable FFL lens.

Sony alpha a5100		Sony FE 35mm F2.8 ZA Carl Zeiss T Lens	
			
Max resolution	6000 x 4000	Lens type	Prime lens
Image ratio w:h	3:2, 16:9	Focal length	35 mm
Effective pixels	24 megapixels	Lens mount	Sony FE
Sensor size APS-C	(23.5 x 15.6 mm)	Aperture	F2.8 - F22
Sensor type	CMOS	Minimum focus	0.35 m (13.78")
Digital zoom	Yes (2X (Clear Image Zoom), 4X (digital zoom))	Maximum magnification	0.12x
Manual focus	Yes	Weight)	120 gram
Focal length multiplier	1.5x	Diameter	62 mm (2.44")
Max shutter speed	1/4000 sec	Length	37 mm (1.46")
Weight (include batteries)	283 gram		

The fixed-wing UAV used for flight missions is hobby grade aeromodelling equipped with a low cost single frequency GPS receiver supporting Global Navigation Satellite System Precise Point Kinematics (GNSS-PPK) [25]. It enables Autopilot system to control aircraft maneuver automatically as well as distance interval for the camera's shutter release precisely. Flight missions are carried out at around 250m flying height above the ground controlled by a navigational grade avionic sensor on board to provide sensor spatial resolution of GSD at about 27mm with a forward overlap and side lap constitute 80% and 60% respectively. In every flight missions for photographing purposes, the camera is mounted to a fixed wing body with a nadir view looking, and one flight mission covers an area of about 300Ha. Topographic variations of the area are spanning from flat ground to moderately undulated terrain.

To meet the ASPRS standards of accuracy assessment, two test fields are designed in the project area. The first test field area consists of an array around 30 control points laid out regularly on the relatively flat terrain which has small elevation differences of approximately 30cm (Figure 2a), meanwhile the second test field comprises about 30 control points over 50m elevation differences (Figure 2b), constituting approximately 20 per cents of average flying height above terrain. These control points are measured using GPS-RTK to give 3D coordinates with an accuracy of about 1cm, and they are applied as an independent check points (ICP). These number of checkpoints are surpassed the ASPRS requirements for a minimum number of checkpoints for an area of about 5000Ha [30]. For registration purposes, there are about 20 ground control points (GCPs)

located and distributed within the whole project area and their coordinates measured by geodetic type of GPS and it gives an accuracy of about 2mm.

The control points are made up from a retro target (Figure 2c and Figure 2d) that of a white concentric ring surrounded with dark background to facilitate a possible highest accuracy of image coordinate measurements of control points on images [10]. These retro targets are served as GCPs and ICPs on the field and they are tools for accuracy controls of the orthophoto as well as facilitating camera self-calibration [6, 8]. While the GCPs are measured using a rapid static mode of the geodetic type GPS measurements, the ICPs control points coordinates are measured using GPS-RTK to an accuracy of about 1cm. However, these control points coordinates are much more accurate than that of the GPS PPK measurements on board.

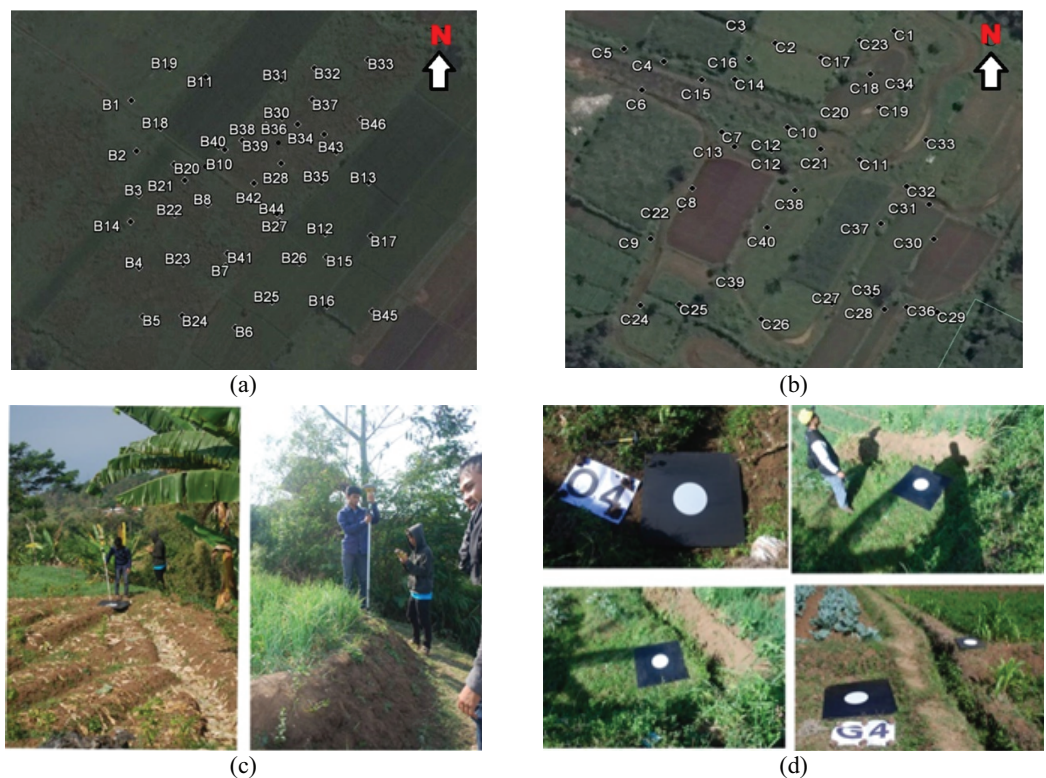


**Figure 2:** (a). The first test field: 40 ICPs over a flat, (b). the second test field: 50 ICPs over a slanted and rugged terrain, (c). some GCPs placements, (d). GPS RTK measurements of ICP's retro target.

### 3. Results and Discussion

When the flight mission covers the ICPs test field area (Figure 2a and Figure 2b), the mission is repeated once again for crossing previous flight courses to facilitate in-flight camera calibration using redundant flight paths [6, 8]. The calibration result is presented in Table 2.

TABLE 2: Camera calibration parameters.

Parameters	c (mm)	x <sub>0</sub> (mm)	y <sub>0</sub> (mm)	K <sub>1</sub>	K <sub>2</sub>	K <sub>3</sub>	P <sub>1</sub>	P <sub>2</sub>	b <sub>1</sub>	b <sub>2</sub>
Values	35,84	-0,0726	-0,4469	2,05E-05	-7,01E-8	7,92E-10	2,38E-06	5,07E-05	-1,38E-4	-2,90E-4

There are more than 50,000 aerial images collected during the campaign and they are processed by using Agisoft PhotoScan software. A workflow of this software is accomplished in three distinct steps. The first stage is the alignment of images by feature identification and matching by setting an accuracy choice to high. The outcome of this stage is the EO parameters of each image, the internal calibration parameters (Table 1), and 3D coordinates of sparse point clouds of the terrain. In the next stage, densification of the generated sparse point clouds is accomplished by using the height field method which is based upon hybrid of pairwise depth-map computation [29] and the MVS stereopsis method [36]. A more detailed 3D model is achieved that could be used to identify the GCPs for aligning the model to the GPS coordinate system. The bundle adjustment is carried out using all the measured GCPs. The last stage is of texturing and meshing processes using the once geo-referenced point clouds in the previous stage. The orthorectification process is done in this stage including radiometric balancing and seamline detection and correction process. The generated orthophoto mosaic comprises of about 169992 x 138191 pixels with resolutions are of 5cm (Figure 3). To ascertain the ability of the software can handle occluded areas on the orthophoto mosaic, a quick visual checking is done and illustrated in Figure 4.

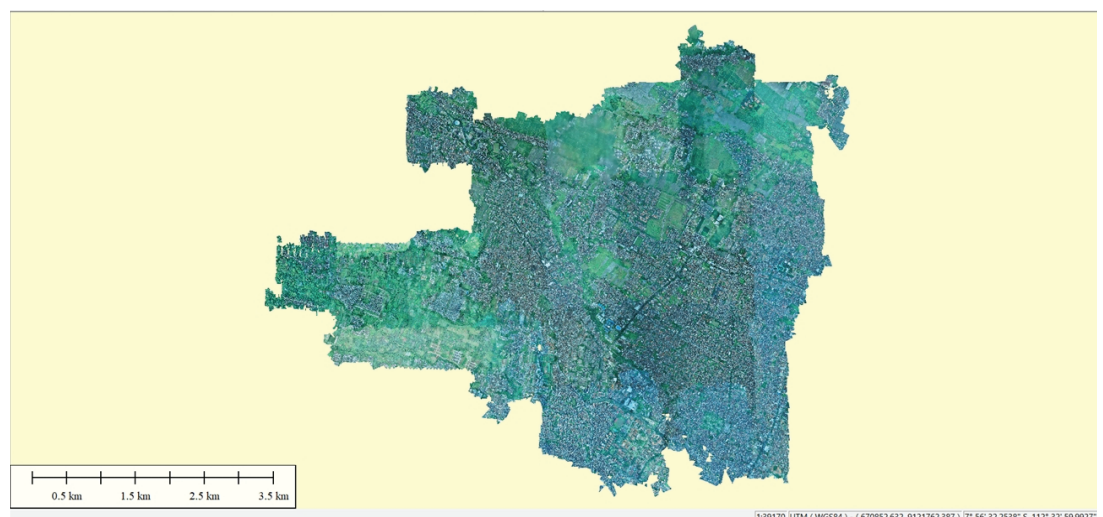
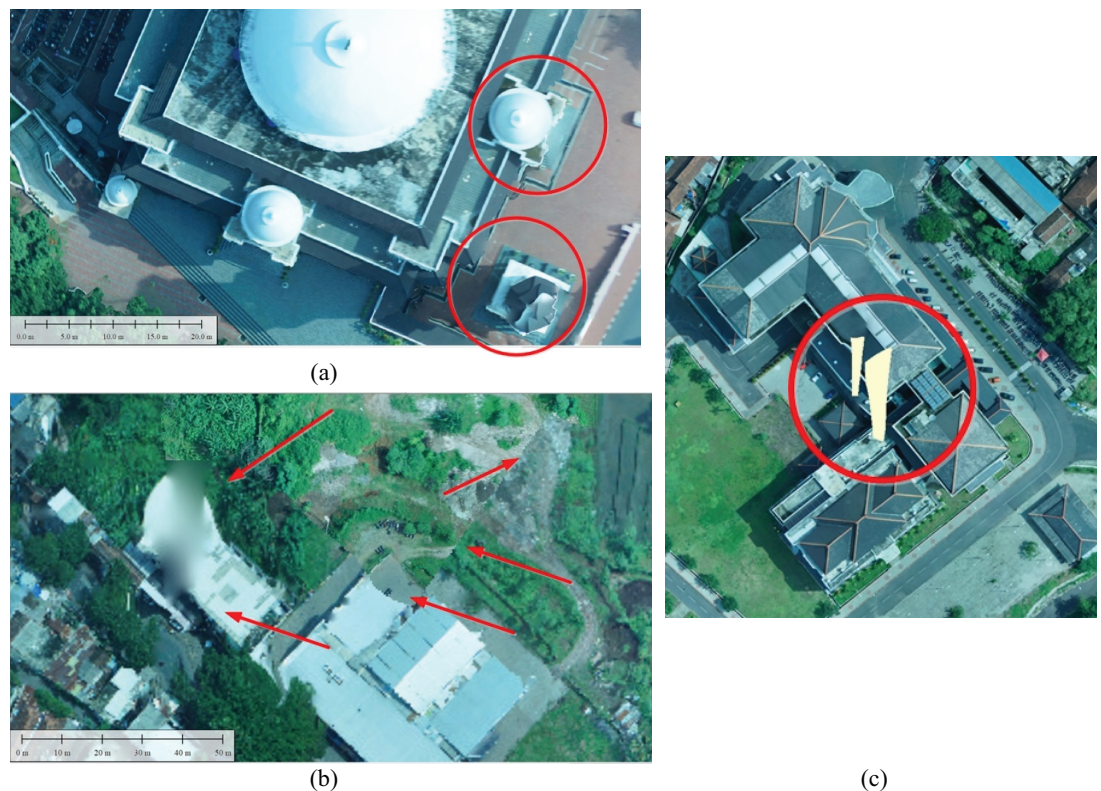


Figure 3: Orthophoto mosaic of Lowokwaru district.



**Figure 4:** Visual check of orthophoto mosaic: (a). errors and noises on the DSM produce artefacts on the elevated man-made object such as building, (b). unresolved seamlines and radiometric unbalanced color intensity values, (c). blank spot area of unknown error.

Figure 4 shows that the accuracy of the orthophoto mosaic is influenced by the quality of the generated DSM (Figure 4a). It seems that the SfM and MVS methods put much attention to a process of automation on a large number of images, neglecting a process called uncertainty error checking in photogrammetric term for more precise point clouds generation to avoid blank spot area (Figure 4c). More over seam line detections and corrections as well as radiometric balancing methods are not working properly for large number of images particularly when the flight mission was conducted on different days with different weather condition (Figure 4b).

Finally, the geometric accuracy of the orthophoto mosaic is evaluated against the ASPRS standard first edition-version-1 2014 [30]. This standard replaces the existing ones and includes positional accuracy standard for orthoimagery. To apply this standard, two test fields on which each contains an array of ICPs across over an area of around 300Ha (Figure 2) are setup inside the project area. A normal flight mission is run using a configuration of 80% of overlap and 60% of sidelap and it covers an area of about 350Ha on the ground. Meanwhile a cross flight mission is termed for a flight paths arranged perpendicularly with the previous flight mission path covering the same area. For the accuracy assessment purposes, aerial photographing is running twice for the

normal and cross flight mission when the UAV flying over the test fields. The RMSE<sub>x</sub>, RMSE<sub>y</sub>, RMSE<sub>r</sub>, and RMSE<sub>r</sub> at 95% percentile according the ASPRS standards 2014 [30] are illustrated in Table 3 as follows.

TABLE 3: Computation of Root Mean Square Error (RMSE) between the ICPs appeared on the orthophoto mosaic and surveyed on the field. All units are expressed in centimeter.

	Field Test 1 (Flat Terrain)		Field Test 2 (Slopped and Rugged Terrain)	
	Normal flight mission	Combination of Normal & Cross flight mission	Normal flight mission	Combination of Normal & Cross flight mission
RMSE <sub>x</sub>	5.13	3.96	10.78	5.35
RMSE <sub>y</sub>	9.10	3.47	10.08	6.88
RMSE <sub>r</sub>	10.45	5.27	14.76	8.72
RMSE <sub>r</sub> at 95%	18.08	9.12	25.55	15.09

Table 3 shows that the orthophoto mosaic that mapping a flat terrain gives better planimetric accuracy than that of an undulated terrain for both normal and combined flight missions in terms of lower RMSE<sub>r</sub>. But the combined flight missions yield better positional accuracy for any kinds of terrain morphologies. Using a combination of normal and cross flight mission is very likely to increase horizontal accuracy by almost two times. Further assessments of the horizontal accuracy of the generated orthophoto mosaic are now compared against Table B5, and Table B6 in the ASPRS standards [30].

According to Table B5, the 5cm per pixel resolution of the generated orthophoto indicates a recommended horizontal accuracy class range of RMSE<sub>x</sub> and RMSE<sub>y</sub> is on the range of equal or less than 5cm, at 10cm, and equal or above than 15cm for categorizing as the highest accuracy work, standard mapping and GIS work, and visualization and less accurate work. Table 3 shows that the RMSE<sub>x</sub> and RMSE<sub>y</sub> from normal flight mission are just suitable for standard mapping and GIS work and for visualization only for any kinds of terrain contours. However, when the combined flight missions are incorporated a much better accuracy can be obtained that it can be used for highest accuracy work applicable for flat and rugged terrains.

According to Table B6, on the flat terrain test field area the value of RMSE<sub>r</sub> (10.45cm) for the normal flight mission and the value of RMSE<sub>r</sub> (5.27cm) for the combined flight mission indicate to an equivalent map scale in 1:300 and 1:200 respectively. On the other hand, on the mountainous terrain the RMSE<sub>r</sub> (14.76cm) for the normal flight mission and the RMSE<sub>r</sub> (8.72cm) for the combined flight mission are suitable for the map scale in 1:500 and 1:300 respectively. However, based upon the GSD of the camera which is 2.7cm, the attainable map scale is up to 1:200 according to the standard. This shows us that uncompensated or partially compensated camera lens distortions and the

IO parameters perturbations can degrade horizontal accuracy as well as an optimum attainable map scales.

## 4. Conclusion

To sum up, overall, a suitable orthophoto mosaic map scale is up to around 1:500 when using consumer grade cameras equipped with a fixed lens system for aerial photogrammetric campaign utilizing UAV. Normal flight path configuration of aerial photography is recommended to produce orthophoto mosaic for standard mapping and GIS work, and for visualization and less accurate work. Horizontal accuracies can be optimized by utilizing a combination of normal and cross flight configurations by a factor of 2 and it is recommended for highest accuracy work using UAV. A provision of test field calibration area and independent check points as well as performing in-flight camera calibration are necessary to achieve optimum map scales.

## Acknowledgement

The authors wish to express their sincere thanks to Ministry of Research, Technology and Higher Education of the Republic of Indonesia for supporting a research grant "Penelitian Terapan Unggulan Perguruan Tinggi (PTUPT)", with a contract number of ITN.03.0376.23/IX.REK/2019.

## References

- [1] P. R. Wolf and B. A. Dewitt. (2000). Elements of Photogrammetry: with Applications in GIS, 3rd ed. *McGraw-Hill Companies Inc., New York*, pp. 217 -- 225.
- [2] E. M. Mikhail, J. S. Bethel, and C. J. McGlone. (2001). Introduction to Modern Photogrammetry. *John Wiley & Sons, Inc., New York*, 2001, pp. 225 -- 238.
- [3] M. Scott. (2013). Photogrammetric Products, in *Manual of Photogrammetry: 6th Edition*, edited by J. C. McGlone. *American Society for Photogrammetry & Remote Sensing, Bethesda, Maryland*, pp. 1009--1043.
- [4] T. J. Blachut and M. C. Van-Wijk, *Photogramm. Eng.* 36, 365--374 (1970).
- [5] G. Konecny, *Photogramm. Eng. Remote Sensing.* 45, 727--734 (1979).
- [6] M. E. Tjahjadi, S. S. Sai, and F. Handoko, "Assessing a 35mm fixed-lens sony alpha-5000 intrinsic parameters prior to, during, and post uav flight mission," in *The 1st*

- International Conference on Geodesy, Geomatics, and Land Administration 2019*, AIP Conference Proceeding, (Accepted).
- [7] B. Altena and T. Goedemé, ISPRS Ann. Photogramm. Remote Sens. Spat. Inf. Sci. **II-5**, 17--24 (2014).
- [8] M. E. Tjahjadi, S. S. Sai, and C. A. Rokhmana, "Assessing stability performance of non-metric camera's lens distortion model during UAV flight missions," in *The 1st International Conference on Geodesy, Geomatics, and Land Administration 2019*, AIP Conference Proceeding, (Accepted).
- [9] M. R. Shortis, S. Robson, and H. A. Beyer, Photogramm. Rec. **16**, 165--186 (1998).
- [10] T. A. Clarke and X. Wang.(1998).Ds And Data Processing For Heat And Fluid Flow.City University,, pp. 311--320.
- [11] K. Novak. (1992).Photogramm. Eng. *Remote Sens.* **58**, 339--344.
- [12] D. Liebowitz and A. Zisserman. (1998).Metric rectification for perspective images of planes, in Computer Vision and Pattern Recognition,*Computer Society Conference on IEEE*, pp. 482--488.
- [13] A. Krupnik. (2003),Photogramm. Rec. **18**, 41--58.
- [14] K. I. Bang and A. F. Habib,. (2007).Comparative analysis of alternative methodologies for true ortho-photo generation from high resolution satellite imagery, in *ASPRS 2007 Annual Conference ASPRS, Tampa, Florida*, pp. 12.
- [15] A. F. Habib, E.-M. Kim, and C.-J. Kim. (2007).Photogramm. Eng. *Remote Sens.* **73**, 025--036.
- [16] L. Barazzetti, R. Brumana, D. Oreni, M. Previtali, and F. Roncoroni. (2014).ISPRS Ann. Photogramm. *Remote Sens. Spat. Inf. Sci.* **II(5)**, 57--63.
- [17] Y. Chen, C. Briese, W. Karel, and N. Pfeifer.(2014) "Int. Arch. Photogramm. Remote Sens. Spat. Inf. Sci. **XL-3**, 67--71.
- [18] G. E. Karras, L. Grammatikopoulos, I. Kalisperakis, and E. Petsa, Photogramm. Eng. *Remote Sens.* **73**, 403--411 (2007).
- [19] M. E. Tjahjadi, F. Handoko, and S. S. Sai. (2017).Int. J. Electr. Comput. Eng. **7**, 1188--1196.
- [20] Q. Chen, M. Sun, X. Hu, and Z. Zhang. (2014).*Remote Sens.* **6**, 12334--12359.
- [21] Z. Maoteng, X. Xiaodong, and Z. Junfeng. (2018).*ISPRS J. Photogramm. Remote Sens.* **138**, 30--46.
- [22] Y. Afek. (1998). Photogramm. Eng. *Remote Sens.* **64**, 115--125.
- [23] C.-H. Lin, B.-H. Chen, B.-Y. Lin, and H.-S. Chou.(2016). ISPRS J. Photogramm. Remote Sens. **119**, 426--436.

- [24] C. A. Rokhmana, M. E. Tjahjadi, and F. D. Agustina, "Cadastral surveys with non-metric camera using UAV: a feasibility study," in *The 1st International Conference on Geodesy, Geomatics, and Land Administration 2019*, AIP Conference Proceeding, (Accepted).
- [25] C. A. Rokhmana, I. A. Gumeidhidta, and M. E. Tjahjadi, "Potential use of uav-based mapping system to accelerate the production of parcel boundary map in Indonesia," in *The 1st International Conference on Geodesy, Geomatics, and Land Administration 2019*, AIP Conference Proceeding, (Accepted).
- [26] G. Esposito, G. Mastrorocco, R. Salvini, M. Oliveti, and P. Starita.(2017).Environ. Earth Sci. 76, 1--16.
- [27] Y. Tan, S. Wang, B. Xu, and J. Zhang.(2018).ISPRS J. Photogramm. Remote Sens.146, 421--429.
- [28] F. Chiabrando, E. Donadio, and F. Rinaudo, Int. Arch. Photogramm. Remote Sens. Spat. Inf. Sci. XL-5/W7, 91--98 (2015).
- [29] F. Agüera-Vega, F. Carvajal-Ramírez, and P. Martínez-Carricondo.(2017). J. Surv. Eng. 143, 4016025.
- [30] ASPRS (American Society for Photogrammetry and Remote Sensing), Photogramm. Eng. Remote Sens. 81, A1--A26 (2015).
- [31] M. E. Tjahjadi and F. Handoko, "Single frame resection of compact digital cameras for UAV imagery," in *Deep Learning High Speed Processing technologies and Its Application on Electrical, Electronics, Computer science and Informatics for Humanity*, 4th International Conference on Electrical Engineering, Computer Science and Informatics (EECSI), edited by M. A. Riyadi et al. (IEEE, Yogyakarta, 2017), pp. 409-413.
- [32] model," in *Achieving Sustainability through Digital Earth*, 2017 International Symposium on Geoinformatic (ISyG), (IEEE, Malang, 2017), pp.19-24.
- [33] M. E. Tjahjad.(2016).ARPN J. Eng. Appl. Sci.11, 3449--3455.
- [34] M. E. Tjahjadi and F. D. Agustina, "A Relative Rotation between Two Overlapping UAV's Images," in *Toward the Next Generation of technology*, 5th International Conference on Electrical Engineering, Computer Science and Informatics (EECSI), edited by A. Yudhana et al. (IEEE, Malang, 2018), pp. 658--663.
- [35] M. E. Tjahjadi and F. D. Agustina.(2019). Int. J. Adv. Intell. Informatics **5**, 24--39.
- [36] A. Mingyao, H. Qingwu, L. Jiayuan, W. Ming, Y. Hui, and W. Shaohua,(2015).Remote Sens. 7, 2302--2333.